THE JOURNAL OF PHYSICAL CHEMISTRY Letters

pubs.acs.org/JPCL Letter

Role of Solvent Rearrangement on Mg^{2+} Solvation Structures in Dimethoxyethane Solutions using Multimodal NMR Analysis

Ying Chen, Nicholas R. Jaegers, Hui Wang, Kee Sung Han, Jian Zhi Hu, Karl T. Mueller,* and Vijayakumar Murugesan*

Cite This: *J. Phys. Chem. Lett.* 2020, 11, 6443−6449 Read Online

ACCESS | Metrics & More | Article Recommendations | Supporting Information

ABSTRACT: One of the main impediments faced for predicting emergent properties of a multivalent electrolyte (such as conductivity and electrochemical stability) is the lack of quantitative analysis of ion−ion and ion−solvent interactions, which manifest in solvation structures and dynamics. In particular, the role of ion−solvent interactions is still unclear in cases where the strong electric field from multivalent cations can influence intramolecular rotations and conformal structural evolution (i.e., solvent rearrangement process) of low permittivity organic solvent molecules on solvation structure. Using quantitative ^{1}H, ^{19}F, and ^{17}O NMR together with ^{19}F nuclear spin relaxation and diffusion measurments, we find an unusual correlation between ion concentration and solvation structure of $Mg(TFSI)_2$ salt in dimethoxyethane (DME) solution. The dominant solvation structure evolves from contact ion pairs (i.e., $[Mg(TFSI)(DME)_{1-2}]^{+}$) to fully solvated clusters (i.e., $[Mg(DME)_3]^{2+}$) as salt concentration *increases* or as temperature *decreases*. This transition is coupled to a phase separation, which we study here between 0.06 and 0.36 M. Subsequent analysis is based on an explanation of the solvent rearrangement process and the competition between solvent molecules and TFSI anions for cation coordination.

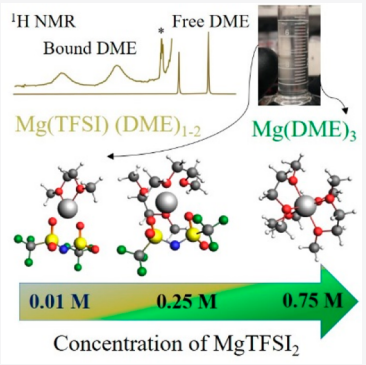

Downloaded via UNIV OF CALIFORNIA BERKELEY on September 18, 2020 at 17:58:44 (UTC).
See https://pubs.acs.org/sharingguidelines for options on how to legitimately share published articles.

With recently growing interest in multivalent batteries, the need for a molecular level view of multivalent ion diffusivity in nonaqueous and aprotic electrolytes has greatly increased.[1−4] However, the complexities associated with solvation phenomena (such as ion pairing and conformal structural evolutions) of multivalent cations and molecular anions in low permittivity solvents is a challenging task. For example, an increase in the number of contact ion pairs (CIPs)—the association of oppositely charged ions—with increasing salt concentration is often invoked as the most plausible explanation of changes in conductivity and viscosity for electrolyte solutions. However, the common Mg^{2+} battery electrolyte system (magnesium bis(trifluoromethanesulfonyl)-imide ($MgTFSI_2$) in a 1,2-dimethoxyethane (DME) solvent) displays a unique concentration dependent phase separation phenomenon and unusual molar ionic conductivity with a maximum observed around 0.6 M followed by a drop in conductivity until the solution is saturated. In addition, the fully solvated $[Mg(DME)_3]^{2+}$-based adduct structure nucleates from near-saturated solutions, which is contrary to the common hypothesis of enhanced ion pairing under higher ionic populations.[5,6] In addition, recent findings from spectroscopic and computational studies suggest that $Mg(TFSI)_2$ in DME exists primarily as fully solvated free ions independent of concentration.[6,7] However, these results are not consistent with the relevant molar conductivity observed in this electrolyte system. Recently, Persson et al. reported that the molar ionic conductivity evolution and Mg^{2+} solvation structure are mainly dictated by increased permittivity due to CIP formation that subsequently leads to fully solvated $[Mg(DME)_3]^{2+}$ at higher concentrations through a redissociation process.[8] The remaining gaps to be explained in the proposed redissociation mechanism are (a) a quantitative description of speciation with ionic strength, and (b) an understanding of the role of conformal structural flexibility of the DME solvent molecules. Interestingly, the redissociation mechanism relies on an increase in the orientational polarizability of CIP species at higher ionic strength, but the effects of increased permittivity on conformal structures and the associated dynamics of flexible DME solvent molecules, as well as unbound TFSI anions, are still unclear.[6−8] For example, hindered intramolecular rotations and conformal structural evolution due to the electrostatic force of Mg^{2+} can bring more solvating sites of DME molecules in contact with Mg^{2+} and compete with TFSI anions. Such compressive structural rearrangements can lead to reduction in volume of the solvent in the Mg^{2+} solvation shell(s) relative to the bulk solution,

Received: May 11, 2020
Accepted: July 16, 2020
Published: July 16, 2020

© 2020 American Chemical Society

https://dx.doi.org/10.1021/acs.jpclett.0c01447
J. Phys. Chem. Lett. 2020, 11, 6443−6449

which is commonly referred as electrostriction.[9] Deeper understanding of this solvent rearrangement process requires delineation of specific interaction between various Mg^{2+} species and solvent/anion molecules. In particular, understanding the structural and dynamic effects of long-range electrostatic interaction between CIPs and solvent molecules can help us explain and predict phase separation phenomena, ionic diffusivity, and solubility limits of multivalent electrolytes. Simultaneously probing the solvation structure and associated dynamics is critical for understanding the role of solvent rearrangement in these low-permittivity electrolyte solutions.[10−12] In order to evaluate the conformal structural flexibility of solvent molecules under electrostriction conditions, we present a quantitative analysis of Mg^{2+} solvation structure and dynamics as a function of salt concentration and temperature using multinuclear NMR spectroscopy.

We prepared $MgTFSI_2$/DME solutions at various concentrations: 0.01, 0.05, 0.1, 0.25, 0.35, 0.4, 0.5, and 0.75 M. The water content is measured using the Karl Fischer titration method and found to be less than 10 ppm for all solutions (see the Supporting Information). Two distinguishable layers at moderate salt concentrations (i.e., 0.1, 0.25, and 0.35 M) are clearly visible, indicating a phase separation as reported by Salama et al.[6] This visually distinguishable phase separation is predominantly driven by changes in preferential molecular solvate structures, as evidenced by a decrease in the relative volume of top layer with an increase in salt concentration. Figure S1 shows the density and viscosity measured at 25 °C as a function of $MgTFSI_2$ concentration. Within the 0.1−0.35 M concentration range, the density of the top layer (0.883−0.890 g/mL) and lower layer (0.992−0.998 g/mL) shows minor changes. Also, the density values of the top and bottom layer correlate well with the values measured at a lower concentration (0.883 g/mL at 0.05 M) and at a higher concentration (1.008 g/mL at 0.4 M) respectively, suggesting common solvation structures are present. The viscosity evolution (Figure S1) also displays similar trends, albeit with different rates of change with salt concentration. The strong electric field of an Mg^{2+} ion can exert a compressive force on the solvent in the solvation shell(s), such that the volume of the solvent in the shell(s) might be smaller than that in the bulk. Such a volume contraction calculated from the measured density of the solution was traditionally used as a measure of electrostriction.[9] However, the challenges in accurate density measurement prevent us from analyzing the electrostriction driven volume contraction in $MgTFSI_2$/DME solutions (see Figure S2). Hence, we employed NMR spectroscopy to access a wide temporal regime (microseconds to seconds) of solvation dynamics along with chemically unique spatial regimes (up to nanometers) of Mg^{2+} solvation shells by interrogating specific isotopes (^1H, ^{19}F, ^{17}O, and ^{25} Mg) with NMR measurements.

Figure 1 shows high resolution ^1H and ^{19}F NMR spectra of the electrolyte solutions at varying salt concentrations measured using a coaxial insert holding the $MgTFSI_2$/DME solution and an outer thin-wall NMR tube hosting 1 v % CF_3COOH (as the ^{19}F reference) and 0.1 v % H_2O (as the ^1H reference) in D_2O (for signal lock), as depicted in Figure S3. On the basis of our previous study[13] and that of Salama et al.[6] on the adduct material of $Mg(TFSI)_2$ and DME as well as the comparison with DFT calculated chemical shifts (Table 1), we assign the four ^1H resonances from left to right to CH_2 and CH_3 of DME coordinated to Mg^{2+} (labeled "bound CH_2" and

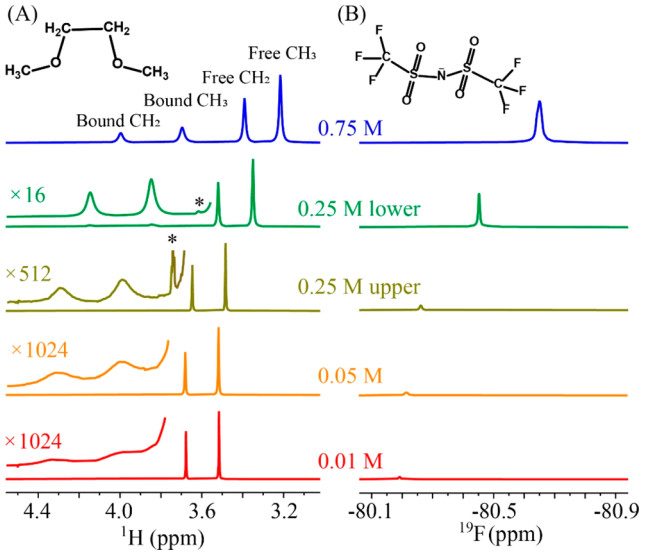

Figure 1. Single-pulse ^1H (A) and ^{19}F (B) NMR spectra of $MgTFSI_2$ in DME at varying concentrations collected at 10 °C. The asterisk * indicates the satellite of the $^{13}CH_2$ resonance from free DME. ^1H spectra are normalized to the highest peak (free CH_3) while ^{19}F spectra are normalized to the signal from the CF_3COOH in the outer sample space (see text).

"bound CH_3") and CH_2 and CH_3 of free DME ("free CH_2" and "free CH_3"). Detailed chemical shift comparisons of experimental and DFT predicted chemical shifts are described in the Supporting Information (Figure S4 and Table S1). With this chemical shift based molecular speciation, the composition of free and bound DME can be directly estimated from ^1H peak ratios. Unlike the solvent molecules, the ^{19}F NMR shows a single resonance representing faster dynamic exchange between different bonding and conformational states of TFSI anions.[13]

The quantitative concentration of TFSI anions in the top and bottom layers from the solutions with original concentrations of 0.1 and 0.25 M are calculated on the basis of a linear relation obtained from the integration ratio with respect to the CF_3COOH signal (Figure 2A). By interpolating the integration ratio values of the upper and lower layers to the calibration curve through linear regression, we obtain a TFSI concentration of 0.06 and 0.36 M for the top and bottom layer, respectively. With the density, molarity, and fraction of free and bound DME estimated from ^1H NMR, we can calculate the molarity of total DME, number of total DME per Mg^{2+}, and number of coordinated DME per Mg^{2+} using the following equations:

$$\text{molarity of total DME} = \frac{\text{density} - \text{molarity of } MgTFSI_2 \times \text{molar mass of } MgTFSI_2}{\text{molar mass of DME}}$$

$$\text{number of total DME per } Mg^{2+} = \frac{\text{molarity of total DME}}{\text{molarity of } MgTFSI_2}$$

$$\text{number of coordinating DME per } Mg^{2+} = \text{number of total DME per } Mg^{2+} \times \text{fraction of coordinating DME}$$

https://dx.doi.org/10.1021/acs.jpclett.0c01447
J. Phys. Chem. Lett. 2020, 11, 6443−6449

Table 1. DFT Predicted Chemical Shift and Experimentally Observed Chemical Shift for 0.01 and 0.75 M of $Mg(TFSI)_2$ in DME Solution[a]

	δ ^{1}H (ppm)		δ ^{19}F (ppm)		δ ^{17}O (ppm)	
molecule	predicted	observed	predicted	observed	predicted	observed
bulk DME	CH_2: 3.69	CH_2: 3.67[b]			−47.0	−21.9
	CH_3: 3.54	CH_3: 3.51[b]				
$[Mg(DME)(TFSI)]^+$	CH_2: 4.37	CH_2: 4.32[b]	−76.16	−80.19	DME: −63.3	DME: −21.9
	CH_3: 4.12	CH_3: 4.07[b]			TFSI: 109.5,[d] 173.3[e]	TFSI: 162.3
$[Mg(DME)_2(TFSI)]^+$	CH_2: 4.08	CH_2: 4.00[c]	−79.70	−80.64	DME: −59.5	DME: −21.8
	CH_3: 3.99	CH_3: 3.69[c]			TFSI: 109.7,[d] 173.5[e]	TFSI: 162.3
$[Mg(DME)_3]^{2+}$	H_2C: 4.25	CH_2: 4.00[c]			DME: −64.2	DME: −21.8
	H_3C: 4.03	CH_3: 3.69[c]				TFSI: 162.1

[a]The site-specific predicted values with respective molecular structure are given in Supporting Information. [b]For 0.01 M $Mg(TFSI)_2$ in DME solution; [c]For 0.75 M $Mg(TFSI)_2$ in DME solution. [d]For oxygens that are coordinating to Mg^{2+}. [e]For noncoordinating oxygens.

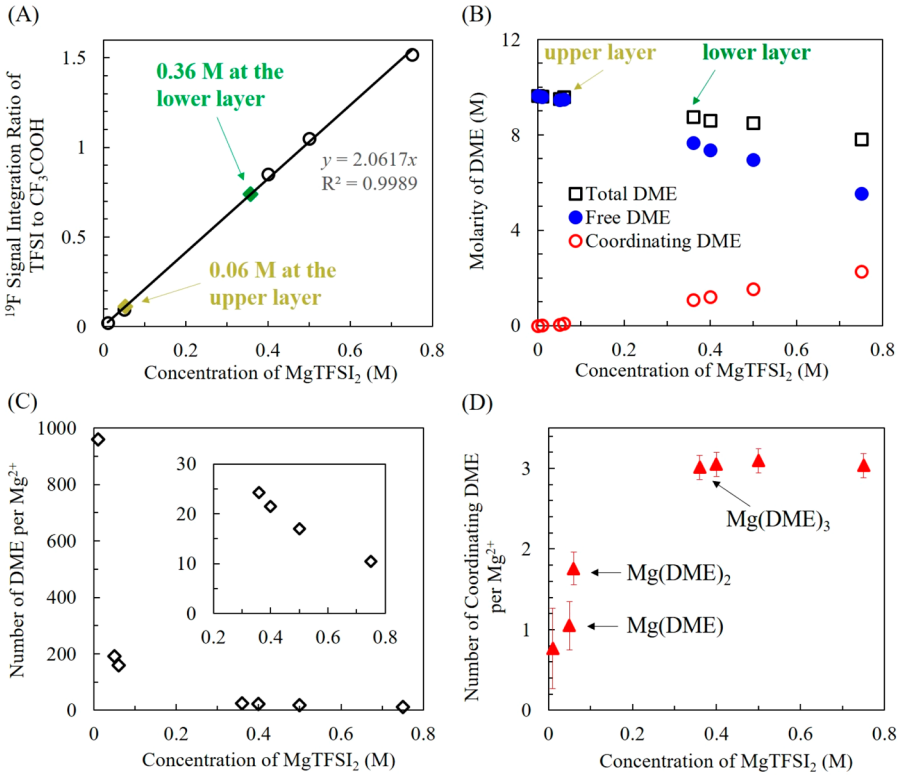

Figure 2. (A) Integration ratio of ^{19}F signal of TFSI to the external reference CF_3COOH plotted against $MgTFSI_2$ concentration. A linear regression of the calibration curve predicts the concentration of the upper and lower layers. (B) Molarity (mol/L) of total DME (black squares), free DME (blue filled circles) and coordinating DME (red circles). (C) Number of total DME per Mg^{2+}. (D) Number of coordinating DME per Mg^{2+} as a function of $MgTFSI_2$ concentration.

While the molarity of total DME decreases gradually with salt concentration (Figure 2B), the number of total DME per Mg^{2+} drops significantly from 960 at 0.01 M to 159 at 0.06 M (upper layer), then dramatically to 24 at 0.36 M (lower phase), and then continuously decreases to 10 at 0.75 M (Figure 2C). More importantly, the number of coordinating DME per Mg^{2+} shown in Figure 2D increases from 0.7 ± 0.5 at 0.01 M to 1.0 ± 0.3 at 0.05 M and 1.6 ± 0.2 at 0.06 M. Nevertheless, the ratio reaches 3.0 ± 0.1 at higher salt concentrations (≥0.36 M) and remains constant until the solution saturates. This observation is contradictory to the assumption by Salama et al. that DME is bound to Mg^{2+} at a constant 3:1 ratio as observed for the crystal adduct of $MgTFSI_2$ in DME.[6] DME has a relatively high Gutmann donor number (19−24 kJ/mol),[14,15] suggesting a stronger affinity to Mg^{2+} and preference for the formation of $Mg(DME)_n$ ($n \leq 3$) clusters. In many studies, the Gutmann donor number has been employed as a useful indicator of the affinity to cation for both anion and solvent.[16,17] However, DME has low density (0.8683 g/mL),[18] low viscosity (0.42 mPa·s),[18] and low permittivity (~7),[8] implying high molecular mobility and a loose molecular packing. Moreover, DME has been shown by Raman spectroscopy[19] to exist as a mixture of five stable conformers in the liquid phase at room temperature, labeled on the basis of local trans (T) and gauche (G) configurations as TGT (42%), TGG′ (33%), TTT (12%), TGG (9%), and TTG (4%). But TGT is the only configuration found in the crystalline adduct of $MgTFSI_2$·3DME,[6] suggesting that TGT is the preferential conformational structure coordinating to Mg^{2+} under suppressed molecular motions. Considering the unique properties

https://dx.doi.org/10.1021/acs.jpclett.0c01447
J. Phys. Chem. Lett. 2020, 11, 6443−6449

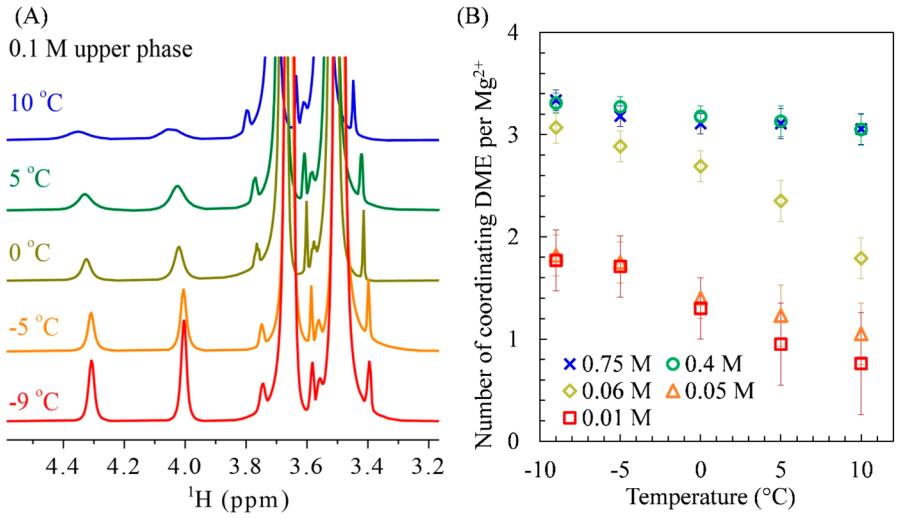

Figure 3. (A) ^{1}H NMR spectra of 0.06 M $MgTFSI_2$/DME at varying temperatures, with each spectrum normalized to its highest peak (free CH_3). (B) Number of bound DME per Mg^{2+} at varying temperatures and concentrations.

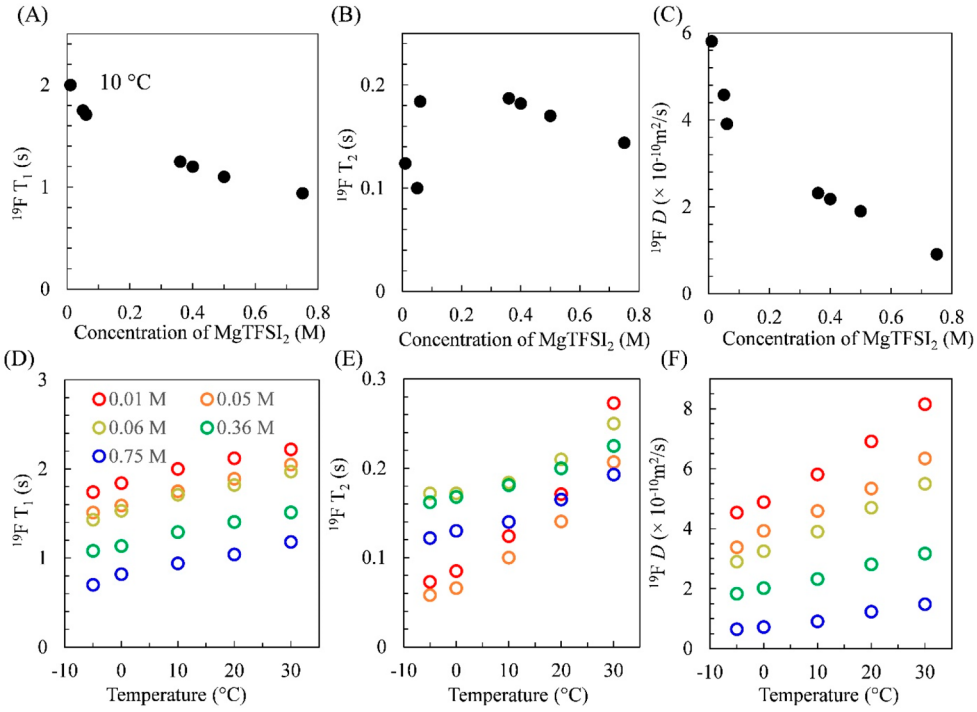

Figure 4. ^{19}F spin−lattice relaxation time T_1 (A, D), ^{19}F spin−spin relaxation time T_2 (B, E), and self-diffusion coefficient D of TFSI (C, F) of $MgTFSI_2$/DME solutions plotted against salt concentration at 10 °C (A)−(C) and plotted against temperature (D)−(F).

of DME, we propose that at lower salt concentrations, the average greater distance between Mg^{2+} ions and higher molarity of free DME molecules render effective screening of the electrostatic interaction. This condition leads to lower electrostriction and diminished entropy loss at lower salt concentrations, eventually favoring loosely associated clusters $Mg(DME)_n$ ($n \leq 2$) owing to the higher degree of freedom and structural flexibility of DME. In contrast, at higher salt concentrations, the shorter distance between Mg^{2+} ions can enforce stronger electrostatic interactions and dampened molecular motion of DME due to enhanced electrostriction and higher entropy loss.[10] Under these combined spatial and dynamic restrictions, DME molecules will obtain the TGT confirmation where two oxygen from each DME bind with a Mg^{2+} cation (bidentate configuration) to form relatively stable fully solvated cluster $[Mg(DME)_3]^{2+}$ with TFSI anions located in the secondary solvation shell. These more densely packed nanoscale solvation structures driven by electrostrictive volume contraction (i.e., the creation of locally higher density) may initiate phase separation and become part of bottom layer in the solution. This putative electrostatic-driven solvent rearrangement can also be probed by lowering the temperature of the solution, such that entropic factors including vibrational, rotational and translational motion of solvent molecules can be further suppressed.

The ^{1}H NMR resonances of DME molecules show line narrowing (due to the slower exchange between bound and free DME) and gradual increase in fraction of bound DME in

https://dx.doi.org/10.1021/acs.jpclett.0c01447
J. Phys. Chem. Lett. 2020, 11, 6443−6449

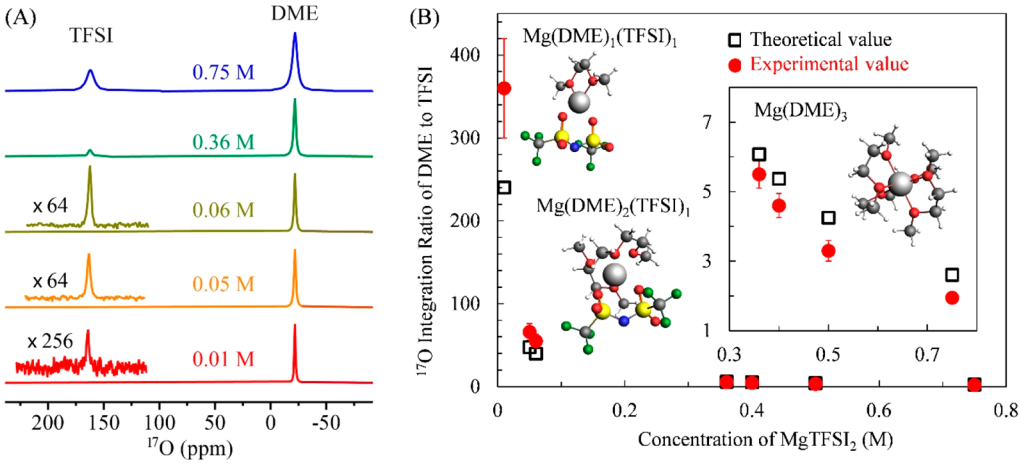

Figure 5. (A) ^{17}O NMR spectra of $MgTFSI_2$/DME solutions at 10 °C. (B) ^{17}O integration ratio of total DME to TFSI. The red circles are experimental values and the black square are calculated values based on the molarity of total DME and TFSI.

the temperature range from +10 °C to −9 °C (Figure 3). The DME coordinating number at higher concentrations (0.4 and 0.75 M) slightly increases from 3.0 ± 0.2 at 10 °C to 3.3 ± 0.1 at −9 °C. Remarkably, the coordinating number increases from 1.8 ± 0.2 to 3.1 ± 0.1 at 0.06 M. Even for lowest concentration (i.e., 0.01 M), the DME coordinating number doubles from 0.7 ± 0.2 to 1.8 ± 0.1 with a decrease in temperature. This overall increase in solvent coordinating number clearly demonstrates that reducing DME mobility drives molecular reorganization to the TGT configuration and subsequently favors fully solvated $[Mg(DME)_3]^{2+}$ clusters.

To probe and understand the role of TFSI anion mobility during the structural evolution of the solvent, we measured ^{19}F NMR spin−lattice relaxation times (T_1), spin−spin relaxation times (T_2), and self-diffusion coefficients (D) for TFSI as a function of salt concentration and temperature. The main relaxation mechanism of the ^{19}F spin−lattice relaxation in TFSI is spin rotation of the terminal CF_3 groups, whereas the ^{19}F spin−spin relaxation of CF_3 group is determined by the chemical exchange rate between multiple sites/conformal structures and the tumbling reorientation of TFSI. Evidently, the monotonic decrease of ^{19}F T_1 with salt concentration correlates with the trend of solution viscosity, reflected in hindered rotation of the CF_3 group (Figure 4A). Similarly, at higher concentrations (≥0.36 M), the measured ^{19}F T_2 values decrease with concentration since TFSI exists mostly in the free anion state with Mg^{2+} preferentially coordinated in fully solvated clusters. Conversely, smaller T_2 values for ≤0.06 M suggest that the restricted molecular motion due to the formation of contact ion pair $Mg(DME)_n(TFSI)_m$ (n, m = 1, 2) and faster chemical exchange between free TFSI and the associated TFSI (Figure 4B). This assumption is supported by a significant drop in self-diffusion constant of the TFSI anion from 0.01 to 0.06 M (Figure 4C) that can be ascribed to the formation of $Mg(DME)_n(TFSI)_m$ clusters. Furthermore, examination of the slopes of ^{19}F T_2 and D behaviors as a function of temperature (Figure 4E,F) reveals a greater change at lower concentrations (0.01, 0.05, and 0.06 M) than at higher concentrations (0.36 and 0.75 M), indicating that the local structure of TFSI evolves from contact ion pairs to free anions in the solution.

As both the anion and solvent coordination with Mg^{2+} happens through oxygen centers (primarily due to their lone pair electrons), the ^{17}O NMR could provide a valuable insight into the evolution of solvation structure. The ^{17}O NMR spectra obtained at all $MgTFSI_2$/DME concentrations (from 0.01 to 0.75 M) display two resonances, at −21.8 and +162.2 ppm, representing DME and TFSI molecules, respectively. The positions of these resonances are invariant across the entire concentration range, while the DFT-calculated ^{17}O chemical shifts are upfield shifted up to 16 ppm for bound DME and 64 ppm for bound TFSI (Table 1). The absence of ^{17}O NMR signals of bound DME and TFSI species may be due to the large quadrupolar coupling constant (QCC) associated with highly asymmetric local environment of bound DME and TFSI anions. The absence of bound TFSI and DME in ^{17}O NMR can be confirmed from quantitative calculations. The theoretical oxygen ratio of DME to TFSI in the solution, i.e. (molarity of total DME × 2)/(molarity of $MgTFSI_2$ × 2 × 4), and the ^{17}O peak integration ratio are plotted as a function of $MgTFSI_2$ concentration in Figure 5B. When assuming all TFSI anions are free at ≥0.36 M, we obtained the bound DME to Mg^{2+} ratio of 2.9 ± 0.2, which is consistent with ^{1}H NMR. With the molarity of free DME obtained from ^{1}H NMR, the bound TFSI to Mg^{2+} ratio is calculated to be 0.5−0.7 at lower concentrations (≤0.06 M), indicating that 25−35% of TFSI exists as CIP based clusters. Note that NMR results reflect an ensemble average of all configurations present in the solution, the most reasonable CIP clusters that agree with ^{1}H, ^{19}F, and ^{17}O NMR results are $[Mg(DME)(TFSI)]^+$ at 0.01−0.05 M and $[Mg(DME)_2(TFSI)]^+$ at 0.06 M. This further confirms that the CIP based clusters are favored at lower concentrations. Considering the significantly lower Gutmann donor number of TFSI (5.4 kJ/mol)[20,21] compared to DME (19−24 kJ/mol),[14,15] we expect to have fully solvated clusters $[Mg(DME)_3]^{2+}$ as the dominant species at lower concentrations due to the abundance of DME molecules. However, as multinuclear NMR studies have revealed, we must consider the retardation of solvent mobility due to electrostriction along with structural flexibility of solvent and anion molecules in predicting the solvation structural evolution. As a low-viscosity and low-permittivity solvent, weaker intermolecular interactions between the DME molecules enable fast exchange between conformal states thereby impeding the bidente coordination needed for $[Mg(DME)_3]^{2+}$ formation. As salt concentration increases, the enhanced electrostatic interactions

https://dx.doi.org/10.1021/acs.jpclett.0c01447
J. Phys. Chem. Lett. 2020, 11, 6443−6449

can force DME molecules to slow down and have enough time to adjust to an optimum TGT configuration to fully coordinate with Mg^{2+} due to its much higher donor number and thereby push TFSI out of the first solvation shell. Conversely, due to its larger hydrodynamics radius and stronger electrostatic interaction with Mg^{2+}, TFSI has relatively lower mobility, which subsequently facilitates CIP formation even with the higher solvent ratios found under low concentration conditions. It should be noted that the Mg^{2+} ions typically prefer six-coordinated structures at higher concentrations of $MgTFSI_2$ in glyme-based solvents.[22−24] However, the solvation structure of Mg^{2+} is highly dynamic, where the rates of ligand exchange processes (either solvent or TFSI molecular exchange with bulk solution) can lead to time-averaged coordination numbers that would depend on the free energy landscape modulated by the chemical composition and system temperature.[25] The lower coordination number (<6) derived from NMR analysis of 0.01 M solutions indicates that the $[Mg(DME)_1(TFSI)_1]^+$ cluster could exist as a transient state due to faster dissociative ligand exchange processes (see Scheme S1). Further experimental and theoretical studies are ongoing to analyze these ligand exchange mechanisms and their ultimate effects on Mg^{2+} solvation structure and chemical properties.

In conclusion, quantitative ^1H, ^{19}F, and ^{17}O NMR together with ^{19}F NMR relaxation and diffusion of $MgTFSI_2$/DME solutions together demonstrate the transition from CIP-based clusters $[Mg(DME)(TFSI)]^+$ and $[Mg(DME)_2(TFSI)]^+$ at low salt concentrations (≤0.06 M) to fully solvated $[Mg(DME)_3]^{2+}$ at higher concentrations (≥0.36 M). The phase separation between 0.06 and 0.36 M is the result of competition between TFSI and DME to coordinate with Mg^{2+}, leading to separate solvation regimes: TFSI forms CIPs when DME is highly mobile and loosely packed; DME has a much stronger affinity to Mg^{2+} with a preferred conformer TGT when dynamics are reduced, yielding a higher-density region with more densely packed DME and fully coordinated Mg^{2+}. This liquid miscibility gap may be also present in other multivalent electrolytes when salt anion and solvent molecules have significantly different donor number, structural flexibility, and mobility. In particular, the solvent rearrangement in the vicinity of Mg^{2+} cations dictate the molecular mobility and conformal structures of electrolyte constituents and subsequently influences the evolution of solvation structure. It is also quite interesting to note that solvent rearrangement and associated electrostriction processes within the electrode−electrolyte interphase region can be significantly divergent from bulk liquid behavior and could dictate (de)solvation processes and associated electrochemical stability.

■ ASSOCIATED CONTENT

Supporting Information

The Supporting Information is available free of charge at https://pubs.acs.org/doi/10.1021/acs.jpclett.0c01447.

Density and viscosity of $MgTFSI_2$/DME solutions at varying concentrations; apparent molar volume of $MgTFSI_2$ in DME vs salt concentration; experimental methods; computational methods; summary of experimental ^1H and ^{19}F chemical shifts; ^1H, ^{19}F, ^{25}Mg, and ^{17}O chemical shifts of several clusters from DFT calculations; ^1H NMR spectra of bound DME and $^{13}CH_2$ satellite peak of free CH_2; ^{25}Mg NMR spectra; potential dissociative ligand substitution mechanism; impurities in $MgTFSI_2$/DME solutions (PDF)

■ AUTHOR INFORMATION

Corresponding Authors

Karl T. Mueller − *Physical and Computational Sciences Directorate, Pacific Northwest National Laboratory, Richland, Washington 99352, United States; Joint Center for Energy Storage Research (JCESR), Lemont, Illinois 60439, United States;* orcid.org/0000-0001-9609-9516; Phone: (509) 371-6550; Email: Karl.Mueller@pnnl.gov

Vijayakumar Murugesan − *Physical and Computational Sciences Directorate, Pacific Northwest National Laboratory, Richland, Washington 99352, United States; Joint Center for Energy Storage Research (JCESR), Lemont, Illinois 60439, United States;* orcid.org/0000-0001-6149-1702; Phone: (509) 371-6540; Email: Vijay@pnnl.gov

Authors

Ying Chen − *Physical and Computational Sciences Directorate, Pacific Northwest National Laboratory, Richland, Washington 99352, United States; Joint Center for Energy Storage Research (JCESR), Lemont, Illinois 60439, United States;* orcid.org/0000-0001-7417-0991

Nicholas R. Jaegers − *Physical and Computational Sciences Directorate, Pacific Northwest National Laboratory, Richland, Washington 99352, United States;* orcid.org/0000-0002-9930-7672

Hui Wang − *Physical and Computational Sciences Directorate, Pacific Northwest National Laboratory, Richland, Washington 99352, United States; Joint Center for Energy Storage Research (JCESR), Lemont, Illinois 60439, United States;* orcid.org/0000-0003-1997-2312

Kee Sung Han − *Physical and Computational Sciences Directorate, Pacific Northwest National Laboratory, Richland, Washington 99352, United States; Joint Center for Energy Storage Research (JCESR), Lemont, Illinois 60439, United States;* orcid.org/0000-0002-3535-1818

Jian Zhi Hu − *Physical and Computational Sciences Directorate, Pacific Northwest National Laboratory, Richland, Washington 99352, United States; Joint Center for Energy Storage Research (JCESR), Lemont, Illinois 60439, United States;* orcid.org/0000-0001-8879-747X

Complete contact information is available at: https://pubs.acs.org/10.1021/acs.jpclett.0c01447

Notes

The authors declare no competing financial interest.

■ ACKNOWLEDGMENTS

This work was supported by the Joint Center for Energy Storage Research (JCESR), an Energy Innovation Hub funded by the U.S. Department of Energy, Office of Science, Office of Basic Energy Sciences (BES). The authors thank Dr. Krisitn Perrson and Julian Self-for valuable discussions and comments on the original manuscript. A portion of the research was performed using EMSL (grid.436923.9), a DOE Office of Science User Facility sponsored by the Office of Biological and Environmental Research. PNNL is a multiprogram national laboratory operated for the DOE by Battelle Memorial Institute under Contract DE-AC06-76RLO 1830.

REFERENCES

(1) Canepa, P.; Sai Gautam, G.; Hannah, D. C.; Malik, R.; Liu, M.; Gallagher, K. G.; Persson, K. A.; Ceder, G. Odyssey of Multivalent Cathode Materials: Open Questions and Future Challenges. *Chem. Rev.* **2017**, *117*, 4287−4341.

(2) Yoo, H. D.; Shterenberg, I.; Gofer, Y.; Gershinsky, G.; Pour, N.; Aurbach, D. Mg Rechargeable Batteries: An on-Going Challenge. *Energy Environ. Sci.* **2013**, *6*, 2265−2279.

(3) Bucur, C. B.; Gregory, T.; Oliver, A. G.; Muldoon, J. Confession of a Magnesium Battery. *J. Phys. Chem. Lett.* **2015**, *6*, 3578−3591.

(4) Song, J.; Sahadeo, E.; Noked, M.; Lee, S. B. Mapping the Challenges of Magnesium Battery. *J. Phys. Chem. Lett.* **2016**, *7*, 1736−1749.

(5) Ha, S.-Y.; Lee, Y.-W.; Woo, S. W.; Koo, B.; Kim, J.-S.; Cho, J.; Lee, K. T.; Choi, N.-S. Magnesium(Ii) Bis(Trifluoromethane Sulfonyl) Imide-Based Electrolytes with Wide Electrochemical Windows for Rechargeable Magnesium Batteries. *ACS Appl. Mater. Interfaces* **2014**, *6*, 4063−4073.

(6) Salama, M.; et al. Unique Behavior of Dimethoxyethane (Dme)/Mg(N(So2cf3)2)2 Solutions. *J. Phys. Chem. C* **2016**, *120*, 19586−19594.

(7) Kubisiak, P.; Eilmes, A. Solvation of Mg2+ Ions in Mg(Tfsi)2−Dimethoxyethane Electrolytes—a View from Molecular Dynamics Simulations. *J. Phys. Chem. C* **2018**, *122*, 12615−12622.

(8) Self, J.; Hahn, N. T.; Fong, K. D.; McClary, S. A.; Zavadil, K. R.; Persson, K. A. Ion Pairing and Redissociaton in Low-Permittivity Electrolytes for Multivalent Battery Applications. *J. Phys. Chem. Lett.* **2020**, *11*, 2046−2052.

(9) Marcus, Y. Electrostriction, Ion Solvation, and Solvent Release on Ion Pairing. *J. Phys. Chem. B* **2005**, *109*, 18541−18549.

(10) Marcus, Y. Electrostriction in Electrolyte Solutions. *Chem. Rev.* **2011**, *111*, 2761−2783.

(11) Marcus, Y.; Hefter, G. Ion Pairing. *Chem. Rev.* **2006**, *106*, 4585−4621.

(12) Marcus, Y.; Hefter, G. Standard Partial Molar Volumes of Electrolytes and Ions in Nonaqueous Solvents. *Chem. Rev.* **2004**, *104*, 3405−3452.

(13) Chen, Y.; et al. Probing Conformational Evolution and Associated Dynamics of Mg(N(So2cf3)2)2·Dimethoxyethane Adduct Using Solid-State 19f and 1h Nmr. *J. Phys. Chem. C* **2020**, *124*, 4999−5008.

(14) Schmid, R. Re-Interpretation of the Solvent Dielectric Constant in Coordination Chemical Terms. *J. Solution Chem.* **1983**, *12*, 135−152.

(15) Brouillette, D.; Perron, G.; Desnoyers, J. E. Apparent Molar Volume, Heat Capacity, and Conductance of Lithium Bis-(Trifluoromethylsulfone)Imide in Glymes and Other Aprotic Solvents. *J. Solution Chem.* **1998**, *27*, 151−182.

(16) Chu, H.; Noh, H.; Kim, Y.-J.; Yuk, S.; Lee, J.-H.; Lee, J.; Kwack, H.; Kim, Y.; Yang, D.-K.; Kim, H.-T. Achieving Three-Dimensional Lithium Sulfide Growth in Lithium-Sulfur Batteries Using High-Donor-Number Anions. *Nat. Commun.* **2019**, *10*, 188.

(17) Horwitz, G.; Factorovich, M.; Rodriguez, J.; Laria, D.; Corti, H. R. Ionic Transport and Speciation of Lithium Salts in Glymes: Experimental and Theoretical Results for Electrolytes of Interest for Lithium-Air Batteries. *ACS Omega* **2018**, *3*, 11205−11215.

(18) Muhuri, P. K.; Hazra, D. K. Density and Viscosity for Propylene Carbonate + 1,2-Dimethoxyethane at 298.15, 308.15, and 318.15 K. *J. Chem. Eng. Data* **1994**, *39*, 375−377.

(19) Goutev, N.; Ohno, K.; Matsuura, H. Raman Spectroscopic Study on the Conformation of 1,2-Dimethoxyethane in the Liquid Phase and in Aqueous Solutions. *J. Phys. Chem. A* **2000**, *104*, 9226−9232.

(20) Linert, W.; Camard, A.; Armand, M.; Michot, C. Anions of Low Lewis Basicity for Ionic Solid State Electrolytes. *Coord. Chem. Rev.* **2002**, *226*, 137−141.

(21) Ue, M. Ionic Radius of (Cf[Sub 3]So[Sub 2])[Sub 3]C[Sup −] and Applicability of Stokes Law to Its Propylene Carbonate Solution. *J. Electrochem. Soc.* **1996**, *143*, L270.

(22) Salama, M.; Shterenberg, I.; Shimon, L. J. W.; Keinan-Adamsky, K.; Afri, M.; Gofer, Y.; Aurbach, D. Structural Analysis of Magnesium Chloride Complexes in Dimethoxyethane Solutions in the Context of Mg Batteries Research. *J. Phys. Chem. C* **2017**, *121*, 24909−24918.

(23) Kitada, A.; Kang, Y.; Matsumoto, K.; Fukami, K.; Hagiwara, R.; Murase, K. Room Temperature Magnesium Electrodeposition from Glyme-Coordinated Ammonium Amide Electrolytes. *J. Electrochem. Soc.* **2015**, *162*, D389−D396.

(24) Shimokawa, K.; Matsumoto, H.; Ichitsubo, T. Solvation-Structure Modification by Concentrating Mg(Tfsa)2−Mgcl2−Triglyme Ternary Electrolyte. *J. Phys. Chem. Lett.* **2018**, *9*, 4732−4737.

(25) Baskin, A.; Prendergast, D. Ion Solvation Spectra": Free Energy Analysis of Solvation Structures of Multivalent Cations in Aprotic Solvents. *J. Phys. Chem. Lett.* **2019**, *10*, 4920−4928.

https://dx.doi.org/10.1021/acs.jpclett.0c01447
J. Phys. Chem. Lett. 2020, 11, 6443−6449